J. Fluid Mech. (1980), *vol.* 96, *part* 4, *pp.* 803–826
Printed in Great Britain

Numerical simulation of thermohaline convection in the upper ocean

By VICTOR E. DELNORE†

Department of Meteorology and Physical Oceanography, Cook College,
Rutgers – The State University of New Jersey, New Brunswick, N.J. 08903

(Received 2 June 1978 and in revised form 29 May 1979)

The intradiurnal heating and cooling cycle of the mixed layer of a tropical ocean is investigated through the use of a 'pseudo-two-dimensional' numerical model. Particular emphasis is given to two-component diffusion resulting from dynamic instabilities in the water column. The conservation equations for salt and heat include the effects of solar heating, horizontal advection and turbulent fluxes at the sea surface, while wind mixing enters through the use of depth-dependent eddy diffusion coefficients resulting from the wave-orbital shear model of Kitaigorodskiy (1961). All inputs are treated as functions of time of day, or calculated via the bulk aerodynamic method.

The entrainment fluxes of salt and heat due to the mechanical stirring of the wind and the fluxes due to molecular diffusion are treated as separate, their respective contributions being added to form the diffusion coefficients used in an alternating-direction explicit scheme to integrate the heat and salt equations. Near the surface, in the absence of strong solar heating (i.e. during the night), these two fluxes alone are insufficient to remove the near-surface static instabilities; thus the presence of some additional process is suggested. A dynamic stability analysis is carried out, based on the temperature and salinity gradients. The resulting Rayleigh numbers indicate the possibility of double-diffusive convection, whereby the vertical transfers of salt and heat may proceed at rates far greater than can be accounted for by molecular diffusion alone. Therefore, the molecular diffusions in the model are increased by a factor roughly proportional to the one-third power of the ratio of the local effective Rayleigh number to a critical Rayleigh number. The modified molecular diffusivities are then added to the eddy diffusion coefficients due to the wind, to form the total diffusion coefficients used in the numerical integrations.

Comparisons are made between the model-generated profiles of temperature and the profiles observed in the ocean. The comparisons show reasonable agreement in the diurnal cycle of the heat wave at 1 m vertical resolution (except for the model-generated surface layer being too deep during the late afternoon hours). (Previous models typically predict only the temperature and thickness of a homogeneous layer.) The results obtained with the model are instructive in estimating the relative importance of the various mixing processes in the upper ocean.

† Present address: Kentron International, Inc., Hampton Technical Center, Hampton, Virginia 23666, U.S.A.

0022–1120/80/4390–8510 $02.00

1. Introduction

Diffusion equations for temperature and salinity are solved numerically, using specified meteorological and radiometric data. The diffusion coefficients are partitioned into a depth-dependent eddy coefficient associated with wind mixing, and an (optional) enhanced molecular diffusion incorporating a Rayleigh number stability criterion to parameterize double diffusion.

The model makes use of previously published methods for determining some of the individual terms in the full diffusion equations, but combines the terms for the first time in numerical experiments for simulating observed upper ocean conditions. Closest agreement between observations and predicted results was obtained when the mechanism of double-diffusive convection was included in the model.

Observations of the mixed layer of the ocean suggest that there are many processes at work, some of them more clearly understood than others. Various models have been formulated in attempts to predict the response of the oceanic mixed layer to changes in meteorological inputs and boundary conditions, for varying initial conditions.

Meaningful reviews of the historical development of mixed-layer models are to be found in Garwood (1977) and in Madsen (1977), with emphasis on depth-dependent vertical eddy viscosity to be found in the latter.

The model developed in the present paper differs from earlier models through the use of double-diffusive convection to augment vertical mixing during periods of marginal stability. This necessitates both a finer vertical resolution and a smaller time step than those used in most previous numerical models. Also, in all the previous models, except that of Miller (1976), no explicit dependence of density on both temperature and salinity was included. This, of course, negates the possibility of static stability being maintained in spite of temperature increasing with depth, a situation observed in the ocean. Instead, the conclusions stated by the authors of many of the cited models contain suggestions that including such salinity dependence and also eliminating the constant eddy diffusion coefficients would lead to improvements in the models. Both suggestions are incorporated in the present formulation, and surface fluxes and volume gains of heat and salt are calculated.

In the model described here, all of the processes known at present to be of importance in shaping the mixed layer's thermohaline structure are included: solar heating, horizontal advection, turbulent fluxes at the sea surface, and wind mixing. All meteorological and radiological inputs are treated as functions of the time of day, or are calculated from empirical formulas. The entrainment fluxes of salt and heat due to the mechanical stirring by the wind and the fluxes due to molecular diffusion are treated separately. Their respective contributions are added to form the diffusion coefficients. A dynamic stability analysis of the water column is carried out, based on the temperature and salinity gradients. The resulting Rayleigh numbers indicate the possibility of double-diffusive convection, whereby the vertical transfers of salt and heat may proceed at rates far greater than can be accounted for by molecular diffusion alone. Therefore, the coefficients of molecular diffusion in the model are increased whenever the Rayleigh numbers satisfy certain criteria to be discussed below. The modified molecular diffusiveness is then added to the eddy diffusion coefficients due to the wind, to form the total diffusion coefficients used in the integrations.

The present study concerns itself with the behaviour of the ocean over several days

at a time, with the emphasis on intradiurnal variations. Seasonal effects are suppressed. Since oceanic soundings are typically obtained on a time scale of hours, the main concern is with processes which contribute to hour-by-hour variations in the observable quantities in the ocean. The meteorological parameters, wind speed, specific humidity, and air temperature, are assumed given. Horizontal currents are not sought as solutions, but are used together with the horizontal gradients of temperature and salinity to calculate horizontal advection. In this sense the model is pseudo-two-dimensional; otherwise the model is one-dimensional. The small compressibility of sea water resulting from hydrostatic pressure is retained in the calculation of density. However, the effects of local pressure variations due to waves are neglected.

2. Water column stability

If the working of the wind and the surface cooling results in a water column with hydrostatic instabilities, then convective overturning must take place to restore stability. Observations indicate that such instabilities must be very short-lived. The potential energy possessed by a statically unstable water column quickly becomes the kinetic energy of the convective motion which restores stability (Turner 1973). The lifetime of the instabilities may be estimated in several ways: the minimum buoyancy period for instabilities in a typical diurnal thermocline of the subtropical ocean is several minutes (Phillips 1966). Ostapoff & Worthem (1974) observed a minimum period of about four minutes for unstable nighttime convection. Shirtcliffe (1969*a*) observed oscillations with periods on the order of one minute in laboratory experiments designed for the study of marginally stable layers.

The vertical gradient of water density is determined by the vertical gradients of both temperature and salinity, if the pressure dependence is neglected. If salinity is held constant, density decreases with increasing temperature. With constant temperature, density increases as salinity increases. If neither temperature nor salinity is held constant (i.e. each is a function of depth) then several possibilities exist for the resulting density profile. For some configurations of temperature and salinity gradients, static stability will result, and, for other combinations, static instability will be the case. Near the limits of static stability, marginal stability exists, and double-diffusive convection may take place. This phenomenon can take one of two forms: (*a*) warm, salty water underlain by cooler, fresher water may give rise to 'salt fingering', thin vertical columns of salty water which descend into the fresher fluid, losing salt and heat as they descend; or (*b*) unstable oscillations may arise on the boundary between cooler, fresher water above warmer, saltier water.

In both cases, the vertical exchange of salt and heat progresses much more rapidly than can be accounted for by molecular diffusion alone. In the absence of the double-diffusive convection or other stability-dependent processes, the mixing would have to be accomplished by wind mixing and molecular diffusion. These may not provide sufficient mixing to remove the static instabilities caused by surface cooling. Double-diffusive convection is an additional exchange process, and this may be the mechanism by which static instabilities are avoided.

Wind mixing and molecular diffusion are normally present at all times; double-diffusive phenomena exist only in the presence of certain combinations of salinity and

temperature gradients. The present model investigates the effect of unstable oscillations, but does not examine cases of salt fingering.

To examine the convective, or dynamic, stability of a water column, it is convenient to define Rayleigh stability numbers for vertically adjacent layers of water. The stability numbers used here are similar in concept to those suggested by Turner (1973). Assuming two layers, one above the other, whose midpoints are Δz apart and whose salinities and temperatures differ by ΔS and ΔT respectively, the following dimensionless numbers may be formed:

$$R_T = \frac{-g\alpha\Delta z^3\Delta T}{\nu K_{mT}}, \tag{1}$$

$$R_S = \frac{g\beta\Delta z^3\Delta S}{\nu K_{mT}}, \tag{2}$$

with $\alpha = -(1/\rho_0)\,\partial\rho/\partial T$ and $\beta = (1/\rho_0)\,\partial\rho/\partial S$. R_T is the thermal Rayleigh number, and R_S is the solutal one. Here g is the acceleration of gravity, ν is the kinematic viscosity of sea water, and K_{mT} is thermal conductivity. (Note that K_{mT} and not K_{mS}, which would be an analogous solutal conductivity, is used in R_S. This is in keeping with the convention of Turner.) The salinity and temperature of the upper layer are S and T respectively, and those of the lower layer are $S+\Delta S$ and $T+\Delta T$ respectively; z is positive downward.

A Rayleigh number for pressure is here defined as

$$R_P = \frac{g\gamma\Delta z^3\Delta P}{\nu K_{mT}} \tag{3}$$

with $\gamma = (1/\rho_0)\,\partial\rho/\partial P$.

From equation (3), γ is eliminated, and R_P is rewritten:

$$R_P = \frac{g\Delta z^3}{\nu K_{mT}}\frac{\Delta P}{\rho_0}\frac{1}{c^2}, \tag{4}$$

where $c = (\partial\rho/\partial P)^{-\frac{1}{2}}$ is the speed of sound in sea water. Now, using $P = \int \rho g\, dz$ and substituting $\partial\rho/\partial z$ for $\Delta p/\Delta z$,

$$R_P = \frac{g\Delta z^4}{\nu K_{mT}}\frac{1}{\rho_0 c^2}\rho g \simeq \frac{g^2\Delta z^4}{\nu K_{mT}}\frac{1}{c^2}. \tag{5}$$

Thus, to a first approximation, R_P depends only on the layer thickness Δz. (Actually, in the numerical calculation, c is calculated explicitly for each depth; the approximation is used here only for the immediate analysis.)

It is seen from these definitions and according to the sign convention used that $R_T > 0$ indicates that the temperature gradient has a stabilizing influence on the density, $R_T < 0$ indicates a destabilizing influence, and $R_T = 0$ implies that the layering has no temperature gradient. The same observations may be made for R_S. $R_P > 0$ always.

A combined thermosolutal Rayleigh number, R_E, may be formed from R_T and R_S:

$$R_E = R_T + \frac{Pr + (K_{mS}/K_{mT})}{Pr + 1} R_S, \tag{6}$$

where Pr is the Prandtl number, defined as ν/K_{mT}, and K_{mS} is the solutal molecular conductivity. $R_E < 0$ shows that the stratification of thc two layers supports a convective instability. Turner & Stommel (1964) identified several modes of mixing in laboratory experiments.

Upper ocean models which treat the density as a function of only the temperature (and, perhaps, also of depth) effectively consider the water stratification to be stable if $R_T \geqslant -R_P$ and unstable otherwise. Including salinity in the density calculation means that the stratification is considered stable for $R_T \geqslant -R_S - R_P$ and unstable otherwise. Thus, as a particular layering configuration progresses from stability to instability, the onset of the instability can be anticipated. The diffusion rates in the model may then be increased accordingly so that the instability can be avoided.

Laboratory experiments by Turner & Stommel (1964), Turner (1965), Shirtcliffe (1969*a*) and Crapper & Linden (1974) have shown that the diffusion rates for heat and salt increase markedly in layering configurations for which double-diffusive convection is indicated. Turner (1965) presents diagrams showing the dependence of the ratio of salt transfer to heat transfer on the net density difference between the layers. Also examined was the dependence of the ratio of upper-layer potential-energy exchange due to salt transfer to that due to heat transfer on the ratio of salt flux to heat flux. In both cases, clear correlations were shown. In the latter case discrete transitions were indicated. Shirtcliffe (1969*b*), using Turner's results and those of his own laboratory experiments, proposed a method whereby the molecular diffusiveness was increased whenever the effective Rayleigh number exceeded a critical value. That method, to be discussed below, allowed prediction of the rapid increase of heat and salt flux rates at the onset of marginal stability, for the unstable convection case.

Occurrences of such phenomena in lakes or oceans have been reported or suggested by Huppert (1972), Huppert & Turner (1972), Ostapoff & Worthem (1974), Gargett (1976) and Newman (1976). Those results, taken together, suggest that, for certain layer configurations in the upper ocean, double-diffusive convection is at work to maintain gravitational stability in the presence of strong surface cooling.

3. Formulation of the model

A fixed, left-handed Cartesian co-ordinate system is used: x, y, and z are defined as positive eastward, northward and downward, respectively. ∇ is the three-dimensional gradient operator. The subscript h denotes the two-dimensional horizontal component of a vector.

The time rates of change of temperature T and salinity S at a point in a column of water, with the neglect of coriolis forces, are given by

$$\frac{dT}{dt} = \nabla.(K_T \nabla \mathbf{T}) + \phi_T, \tag{7}$$

$$\frac{dS}{dt} = \nabla.(K_S \nabla \mathbf{S}), \tag{8}$$

where K_T and K_S are the coefficients of thermal and solutal diffusion, respectively, and ϕ_T is the time rate of temperature change due to all volume sources other than advection. There is no such term for salinity.

Under the assumption of linear horizontal gradients of temperature and salinity, and by neglecting vertical motion and the lateral derivatives of the mixing coefficients, these become

$$\frac{\partial T}{\partial t} = \frac{\partial}{\partial z}\left(K_T \frac{\partial T}{\partial z}\right) - \mathbf{V}_h \cdot (\nabla_h T) + \phi_T, \tag{9}$$

and

$$\frac{\partial S}{\partial t} = \frac{\partial}{\partial z}\left(K_S \frac{\partial S}{\partial z}\right) - \mathbf{V}_h \cdot (\nabla_h S), \tag{10}$$

$\mathbf{V}_h$ is the horizontal current.

The source term for temperature is

$$\phi_T = \frac{1}{c_p \rho} \frac{\partial}{\partial z} Q(z), \tag{11}$$

where $Q(z)$ is the net downward solar energy flux, in cal $\mathrm{cm}^{-2}\,\mathrm{min}^{-1}$, at depth z, c_p is the specific heat of sea water, and ρ is density.

The method for numerical solution of equations (9) and (10) is presented in appendix A.

The upper boundary condition for temperature is

$$K_T \frac{\partial T}{\partial z} = \frac{Q_f}{c_p \rho} \quad \text{at} \quad z = 0, \tag{12}$$

where Q_f is the net flux of heat through the surface, due to evaporation, back radiation, and sensible (conductive) transfer. Heat flux due to precipitation is neglected.

The lower boundary condition for temperature is

$$T = T_0 \quad \text{at} \quad z = D, \tag{13}$$

where T_0 is some fixed temperature, and D is the depth of the lower boundary. D is chosen to be a depth at which both the wave-induced mixing and the solar flux are negligible compared to their surface values, and below which diurnal variations are not important.

The initial condition for heat is

$$T(z) = f_T(z) \quad \text{at} \quad t = 0, \tag{14}$$

where $f_T(z)$ is some known temperature distribution.

The upper boundary condition for salinity is

$$K_S \frac{\partial S}{\partial z} = \left[\frac{Q_e}{\rho L} - \psi\right] S, \tag{15}$$

where S is sea surface salinity, L is the latent heat of evaporation, ψ is the precipitation rate, and Q_e is the evaporative heat flux through the surface. The lower boundary condition for salinity is

$$S = S_0 \quad \text{at} \quad z = D, \tag{16}$$

and the initial condition is

$$S(z) = f_S(z) \quad \text{at} \quad t = 0, \tag{17}$$

where $f_S(z)$ is some known initial salinity distribution. $f_T(z)$ and $f_S(z)$ are determined from oceanic soundings. $\nabla_h S$ and $\nabla_h T$ are treated here as functions of depth but are

held constant in time. Estimates for these quantities can be made for synoptic oceanographic data.

An integration of equation (9) from $z = D$ to $z = 0$ in space, and in time from $t = 0$ to $t = \tau$, and use of the boundary condition of equation (12) yields the integral form of the heat conservation equation.

$$\int_D^0 c_p \rho T \, dz|_{t=\tau} - \int_D^0 c_p \rho T \, dz|_{t=0}$$

$$= \int_0^\tau Q_f \, dt + \int_0^\tau Q \, dt|_{z=0} - \int_0^\tau Q \, dt|_{z=D} - \tau \int_D^0 c_p \rho \mathbf{V}_h . \nabla_h T \, dz. \tag{18}$$

Equation (18) is simply a statement that the heat gained by the water column over a time τ is equal to the time integral of all the sources of heat which are considered. Q is solar heat flux.

An analogous expression for salt conservation may be derived from equation (10):

$$\int_D^0 \rho S \, dz|_{t=\tau} - \int_D^0 \rho S \, dz \, |_{t=0} = \int_0^\tau S\left[\frac{Q_e}{\rho L} - \psi\right] dt - \tau \int_D^0 \rho \mathbf{V}_h . \nabla_h \mathbf{S} \, dz. \tag{19}$$

The surface heat flux Q_f is made up of the flux due to back radiation (Q_b), that due to evaporation (Q_e), and the sensible heat loss to the atmosphere (Q_c). Q_b is calculated according to the method given by Dietrich (1963), and Q_e and Q_c are formulated using methods found in Malkus (1962). The usefulness of these bulk aerodynamic parametrizations has been recently reaffirmed by Friehe & Schmitt (1976).

As latent (evaporative) heat is released from the sea surface at a rate Q_e cal cm^{-2} min^{-1}, the rate of water loss is $Q_e/\rho L$ cm min^{-1}. Even though no salt actually crosses the sea surface (except by second-order processes such as sea spray, ignored here), the evaporation causes an effective downward salt flux rate of SQ_e/L g min^{-1} per cm^2 of ocean surface.

As precipitation takes place at the rate of ψ cm min^{-1}, there is an effective upward salt flux rate of $S\psi\rho$ g min^{-1} per cm^2 of ocean surface. This is due to the decrease in surface salinity as fresh water is added. The net salt flux due to evaporation and precipitation combined is then

$$F_{ep} = S[\psi\rho - Q_e/L]. \tag{20}$$

The total solar flux incident on the sea surface, at wavelength η, is

$$Q'_R(\eta, 0) = Q'_0(\eta) \cos\zeta, \tag{21}$$

where ζ is the complement of solar altitude, and $Q'_0(\eta)$ is the incident flux at wavelength η, from a zenith (directly overhead) sun. A prime (') on a solar flux symbol indicates the flux at a specified wavelength, while the absence of a prime indicates that the flux is the integral over all wavelengths. The net downward solar flux, entering the sea surface after partial reflexion, is

$$Q'(\eta, 0) = Q'_R(\eta, 0)\,(1 - \chi), \tag{22}$$

where χ is the albedo of the sea surface. The net downward flux of solar energy at all wavelengths from η_1 to η_2 is

$$Q(0) = \int_{\eta_1}^{\eta_2} p(\eta)\, Q'(\eta, 0)\, d\eta, \tag{23}$$

where $p(\eta)$ is a weighting function, assumed to be a function of wavelength and not of the amount of solar energy present. From equation (21) and using total attenuation coefficients which are functions of wavelength, and the assumption that the intensity of solar energy at each wavelength is decreased exponentially with depth, the net solar flux at depth z, in the band η_1 to η_2 is determined:

$$Q(z) = \int_{\eta_1}^{\eta_2} p(\eta)\, Q'(\eta, 0)\, e^{-\Gamma(\eta) z} d\eta. \tag{24}$$

$\Gamma(\eta)$ is the total attenuation coefficient for energy at wavelength η, assumed to be the sum of the absorption and the scattering coefficients (Jerlov 1966). From equation (23), the gradient is found:

$$\frac{\partial}{\partial z} Q(z) = -\int_{\eta_1}^{\eta_2} p(\eta)\, \Gamma(\eta)\, Q'(\eta, 0)\, e^{-\Gamma(\eta) z} d\eta \tag{25}$$

$$\simeq \frac{\Delta Q(z)}{\Delta z} = \frac{Q(z+\Delta z) - Q(z)}{\Delta z}$$

$$= \frac{1}{\Delta z} \int_{\eta_1}^{\eta_2} p(\eta)\, Q'(\eta, 0) \left[e^{-\Gamma(\eta)(z+\Delta z)} - e^{-\Gamma(\eta) z}\right] d\eta. \tag{26}$$

Equation (26) is used rather than equation (25) because equation (25) must be evaluated at the midpoint of each layer Δz thick and is not as exact as equation (26) for discrete layer use. Equation (26) actually expresses the difference between the downward solar energy entering the top of a layer and the downward solar energy passing on through the bottom of that layer, and thus more accurately describes the energy used to heat the layer.

The sun's altitude is calculated using standard navigational methods, and the albedo of the sea surface follows from Jacobs & Pandolfo (1974).

4. Thermal and solutal diffusion coefficients

The thermal diffusivity $K_T(z)$ and the solutal diffusivity $K_S(z)$ are both functions of depth. Each is the sum of a wind-induced component, $K_W(u)$, and an augmented molecular component K'_{mT} or K'_{mS}:

$$K_T(z) = K_W(u) + K'_{mT}, \tag{27}$$

$$K_S(z) = K_W(u) + K'_{mS}. \tag{28}$$

The wind-induced component is the same for both K_T and K_S and is calculated through the use of the Kitaigorodskiy (1961) wave-orbital velocity shear model and the assumption that the mixing length varies in proportion to the wave-orbital radius.

The dominant wavelength λ for surface waves in a well-developed sea caused by a wind of $u_{19{\cdot}5}$ cm s^{-1} measured at 19·5 m above the surface (nominal yard-arm height) is, after Pierson (1964),

$$\lambda = 2{\cdot}803 \times 10^{-3} u_{19{\cdot}5}^2 \text{ cm}. \tag{29}$$

From this, the magnitude of the velocity of the orbits of subsurface horizontal wave motion can be found (Kitaigorodskiy 1961):

$$u_{\text{orb}}(z) = \pi\delta[\lambda/2\pi]^{\frac{1}{2}} g^{\frac{1}{2}} e^{-2\pi z/\lambda}, \tag{30}$$

where z is depth and $\delta = 0{\cdot}055$ is the wave steepness for a fully-developed sea. The wind-induced diffusion coefficient is then proportional to the vertical gradient of u_{orb}:

$$K_W(z) = k_1^2(z+\tfrac{1}{2}\delta\lambda)^2\,\partial u_{\text{orb}}(z)/\partial z$$
$$= k_1^2(z+\tfrac{1}{2}\delta\lambda)^2\pi\delta(2\pi g/\lambda)^{\frac{1}{2}}e^{-2\pi z/\lambda}, \tag{31}$$

with $K_W(u)$ now written as $K_W(z)$. k_1 is a constant due to Kitaigorodskiy, $k_1 = 0{\cdot}14$. The value of this constant is not critical.

The above formulation was found by Jacobs (1978) as appropriate for a tropical or subtropical ocean mixed layer under the influence of nearly constant winds. Other models investigated by Jacobs included Richardson number dependence and the discrete exponential model of Mamayev (1958). Jacobs concluded that, for oceanic regions away from boundary currents, the Kitaigorodskiy wave-orbital model is adequate for description of the wind mixing, provided the winds are known.

K'_{mT} and K'_{mS}, the convective, or augmented molecular, components of the total diffusion coefficients, are determined by the method of Shirtcliffe (1969*b*). Using the effective thermosolutal Rayleigh number R_E defined in equation (6), and a critical Rayleigh number $R_{EC} = 1100$ (Palm 1975) for layers bounded by one free and one rigid boundary:

$$K'_{mT} = K_{mT}\left[1+\theta\left(\frac{R_{EM}}{R_{EC}}\right)^{\frac{1}{3}}\left(1-\frac{R_{EC}}{R_{EM}}\right)\right] \quad R_{EM} > R_{EC}, \tag{32}$$

$$= K_{mT} \quad R_{EM} \leqslant R_{EC}; \tag{33}$$

$$K'_{mS} = K_{mS} + K'_{mT} - K_{mT} \quad R_{EM} > R_{EC}, \tag{34}$$

$$= K_{mS} \quad R_{EM} \leqslant R_{EC}. \tag{35}$$

The parameter θ is adjustable and K_{mT} and K_{mS} are the ordinary molecular values for heat and salt diffusion. R_{EM} is the magnitude of the most negative R_E within any contiguous series of layers for which $R_E < -R_{EC}$ in each layer.

The value chosen for θ in equation (32) must provide great enough convective diffusion rates for static instabilities typically found in the ocean to be removed within a time comparable to their observed lifetimes. $\theta = 0$ gives no modification of the molecular values of diffusiveness. Larger values of θ give increased amplification of the molecular diffusivity, thus, in effect, 'speeding up' the diffusion. The results of a numerical experiment to determine the dependence on θ of the time needed to remove typical static instabilities found in the ocean are given in appendix C. Once the convective components of the diffusivity have been determined, they are added to the wind-induced components, as in equations (27) and (28). Through this formulation, the molecular diffusion coefficients are adjusted whenever an unstable convection case is detected. Rayleigh numbers were calculated for the temperature–salinity layerings observed in numerous ocean soundings from Delnore & McHugh (1972), with the result that no cases of salt fingering were found. Likewise, in the numerical simulations presented below, no layerings were generated for which salt fingering would result. For these reasons, salt fingering is not discussed further.

5. Numerical simulations and results

The numerical model was used to simulate the diurnal heating cycle over several days for a subtropical ocean. The meteorological and initial oceanographic conditions were obtained from data gathered on the Barbados Oceanographic and Meteorological Experiment (BOMEX) of 1969. Five ships obtained various meteorological and radiometric data and simultaneously made temperature–salinity–pressure soundings (STD's) several times a day. Synoptic data from all five ships are used here, but oceanic soundings from only the *Discoverer* (location 13° 08′ N, 53° 51′ W) are considered. Descriptions of the hydrography of the BOMEX region may be found in Mazeika (1973), Metcalf (1968) and Ryther, Menzel & Corwin (1967).

Ocean temperatures and salinities were measured with the Plessey Model 9006 multisensor (STD; the term applies to both the instrument and the sounding) unit. Eight soundings were obtained each day: one every three hours around the clock, beginning at 0200 local standard time. (Hereinafter, all times are given as local standard, which for the BOMEX field project was 60° W zone time, or four hours later than GMT.) The STD instrument was lowered from the surface to about 1000 m depth, sampling salinity, temperature, and pressure on the way down but not on the return. Lowering speed through the upper 50 m was 20 m min^{-1}, so that the water between the surface and that depth was sampled in less than three minutes.

From operational records, Delnore (1972) estimated the error in initial depth at the start of each sounding to be $\pm$ 1·5 m. Probable errors in the temperature and salinity measurements are the r.m.s. errors for a single reading of temperature and are expected to be 0·05 °C, and that for salinity 0·03‰.

The solution of equations (9) and (10) provides predictions for salinity and temperature. The finite-difference solution scheme requires certain meteorological and synoptic oceanographic data, and initial vertical distributions of salinity and temperature.

Time-dependent values for wind speed, air temperature, and specific humidity were obtained from Paulson, Leavitt & Fleagle (1972). Values for vapour pressure and saturation specific humidity are from Pandolfo & Jacobs (1972). Cloud cover (0·2) and net downward solar radiation (524·0 cal cm^{-2} day^{-1}) are from Delnore (1972). Depth-dependent horizontal gradients of salinity and temperature, and values for mean horizontal advection were obtained from Pandolfo & Jacobs (1972) and from Sanford (1972).

The initial conditions were constructed by using the observed data from the sounding obtained at 2000, 22 June 1969, with the data below 20 m replaced by the time average of all data observed over the following four days. This modification was done in an effort to suppress the variations in the observed profiles deeper than the bottom of the diurnally mixed layer. These variations are the result of processes not considered in the present model. The vertical interval of the initial data is one metre. An explanation for a near-surface salinity depression is offered in Landis (1971).

Some precipitation did occur during the time the oceanographic data were gathered. Rainfall at sea is difficult to measure, and the BOMEX records, as regards rainfall, are very scanty (Elliott 1974). Therefore, except for one run to be introduced below, the precipitation rate for the simulations was simply set so as to balance the apparent salt flux due to evaporation, i.e.

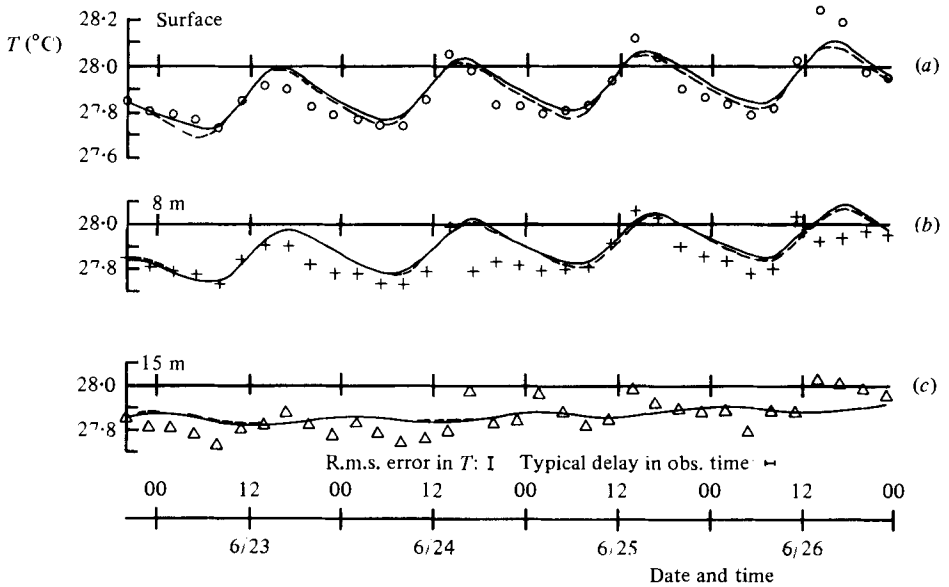

FIGURE 1. Time series of observed (symbols) and predicted (curves) temperature. (*a*) Surface temperature. (*b*) Temperature at 8 m depth. (*c*) Temperature at 15 m depth. Solid curves: runs 1 and 3; broken curves: departures of run 2 from runs 1 and 3. ○, surface; +, 8 metres; △, 15 metres. Upper time scale, time-of-day in hours, local standard time; lower time scale, month and date, 1969.

$$\psi = \rho Q_e / L \tag{36}$$

in equation (15). Thus, the rainfall is proportional to the evaporation and the net salt flux across the sea surface is zero. Any change in the amount of salt in the water column is thus due to horizontal advection.

Three four-day simulations were made, all with identical initial conditions as described above. Run 1 was made with θ, the double-diffusive mixing parameter, equal to 900, and run 2 was made with $\theta = 0$ (no double-diffusive convection). Run 3 was identical to run 1 (i.e. $\theta = 900$), except that the precipitation rate was set to zero. All other input parameters were identical for the three runs.

Over the diurnal cycle, the predicted evaporative salt gain was found to vary between $1{\cdot}08 \times 10^{-5}$ and $1{\cdot}27 \times 10^{-5}$ g cm^{-2} min^{-1}. Horizontal advection causes an apparent salt loss of $3{\cdot}21 \times 10^{-4}$ g cm^{-2} min^{-1}, which is about 30 times that gained through evaporation. For this reason, nearly identical salt gain predictions were generated in runs 2 and 3.

Predicted water temperatures for the four days for runs 1, 2, and 3 are given in figure 1, together with the observed temperatures. The expected r.m.s. uncertainty in the observed data is indicated by error bars. The temperatures predicted in runs 1 and 3 are nearly identical, and are represented by the solid curves in the figure. The broken curves indicate departures of the run 2 temperatures from those of runs 1 and 3. As stated previously, $\theta = 0$ for run 2 and $\theta = 900$ otherwise, and precipitation is set to zero only for run 3. The calculations are successful in predicting the general diurnal cycle and the slight warming trend. At 8 m depth, there is a noticeable phase lag between the predicted and the observed temperature. Apparently the model is slow in its

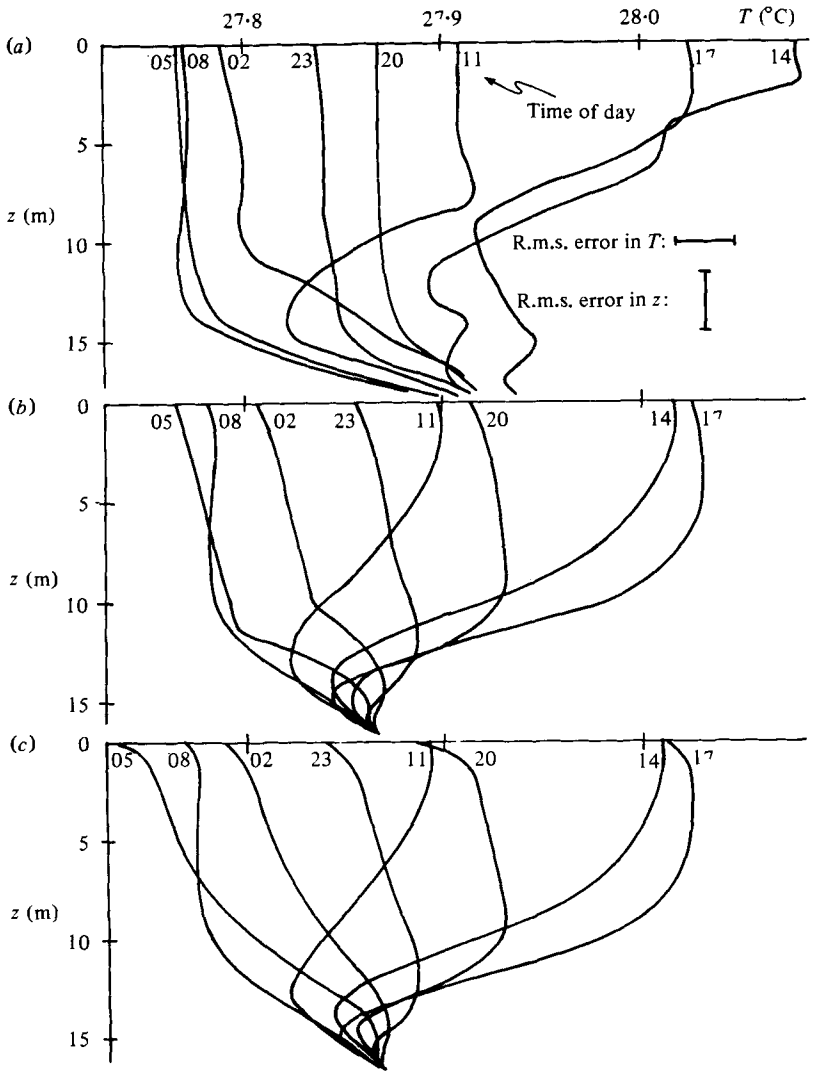

FIGURE 2. Observed and simulated time–temperature profiles. (*a*) Observed data averaged. (*b*) Runs 1 and 3 (θ = 900). (*c*) Run 2 (θ = 0). Small numbers indicate time of day in hours, local standard time.

removal of heat from intermediate depths. Some of the phase lag may be simply the result of delays in starting times of the soundings.

The observed temperature at 15 m depth exhibits no discernible diurnal period. Indeed, the observed temperature variations lie roughly within the limits of the r.m.s. error. Therefore, most of the variation in observed temperature at 15 m may be attributed to noise, which, of course, is not predicted by the model. However, the warming trend apparent in the data is well predicted.

Observed and predicted temperature profiles for each of the standard observation times are shown in figure 2. Each profile is labelled according to time-of-day, local standard time. Only the upper 16 m of the profiles is given. The diffusivity below that

depth is so low that departures of the profiles from those of the initial conditions are insignificant. The integrations were, however, carried to 50 m depth for all simulations. Vertical plotting resolution for all profiles is 1 m.

Temperature profiles obtained by averaging together, by time of day, the observed data for the four days are given in the topmost portion of the figure. The averaging was performed in order to emphasize the diurnal heating cycle in the observations, and to suppress noise, trends, and observational errors. Error bars for both depth and temperature are shown.

Predicted temperature profiles for the second day of run 1 are given in the centre portion of the figure. (The second day is used rather than the first to avoid start-up phenomena. Once the cycle is established, it is repeated.) Profiles from the second day of run 2 ($\theta = 0$) are given in the bottom part of figure 2. The temperature predictions for run 3 (zero precipitation rate) are nearly identical to those of run 1, and thus are not shown separately.

The model predicts the temperature profiles quite well, especially during the warming part of the cycle. The cooling, however, is not nearly as rapid as it should be, as evidenced by the excessive temperature of the simulated profiles for 2000 and 2300. It is obvious that the use of augmented diffusiveness ($\theta = 900$ rather than zero) allows better prediction of the mean profiles. The main differences to be seen between runs 1 and 2 (figures 2*b* and 2*c*, respectively) are that, in the latter case ($\theta = 0$), the nighttime profiles (labelled 20, 23, 02, and 05) are not sufficiently isothermal, and static instabilities are developed in the early morning hours. No such instabilities were generated in runs 1 and 3. Also, the model creates a somewhat deeper layer in the late afternoon than nature does.

Time series of observed and predicted salinity at the sea surface and at 8 and 15 m depth are given in figure 3. The salinity predictions from runs 1 and 2 are shown as solid curves and are identical within the plotting resolution of the figure. The predicted salinity from run 3 (no precipitation) is always slightly greater than that for the other two runs, and is shown in figure 3 by dotted lines.

It is seen that the observed salinity at all three depths exhibits no clearly discernible diurnal pattern; thus it is meaningless to average these data by time-of-day as was done for the observed temperatures. The time history of observed salinity suggests that in the afternoons of both the 24th and 26th of June either heavy precipitation or increased advective salt loss, or some combination of both, took place – it would be difficult from available data to determine which. Since the input data include a precipitation rate set either to zero (run 3) or adjusted to balance the surface salt flux due to evaporation (runs 1 and 2), the predicted salinity merely reflects an overall near-surface salt loss due to horizontal advection. This is apparent in the observed data. Obviously, the importance of including salt as a diffusive component lies not in its diurnal behaviour but rather in its contribution to stabilizing the density so that positive values of dT/dz are allowed.

Figure 4 presents observed and predicted σ_t for the sea surface and for 8 and 15 m depth. The calculated σ_t for run 2 ($\theta = 0$) differs appreciably from that of run 1 ($\theta = 900$) only at the sea surface and only during the early morning hours. Thus for run 2, only the departures from run 1 are shown, and these are shown as dashed curves. Run 3 (zero precipitation rate; $\theta = 900$) yielded values of σ_t which were very slightly greater than those of run 1. The difference increases linearly with time, due to the

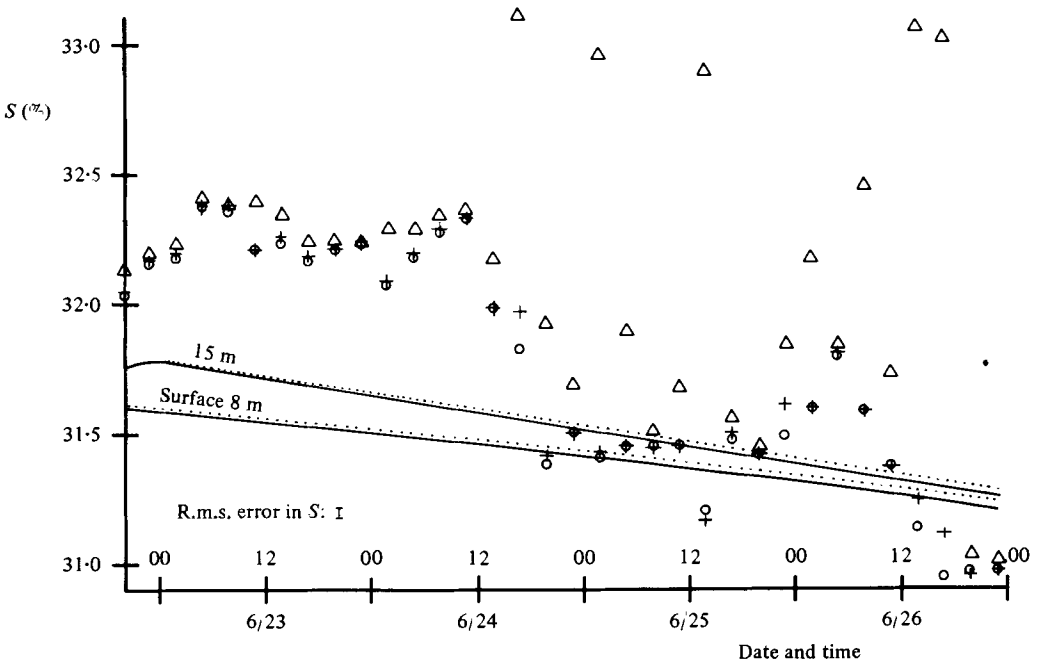

FIGURE 3. Time series of observed (symbols) and predicted (curves) salinity. Time scales are as for figure 1. Solid curves: runs 1 and 2. Dotted curves: run 3. ○, Surface; +, 8 metres; △, 15 metres.

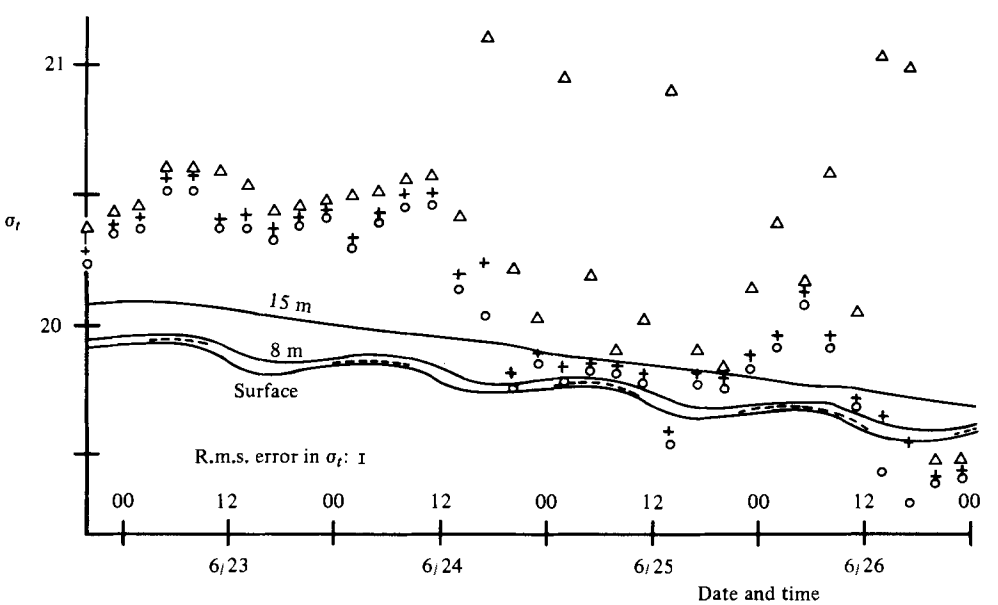

FIGURE 4. Same as figure 1, but for σ_t.

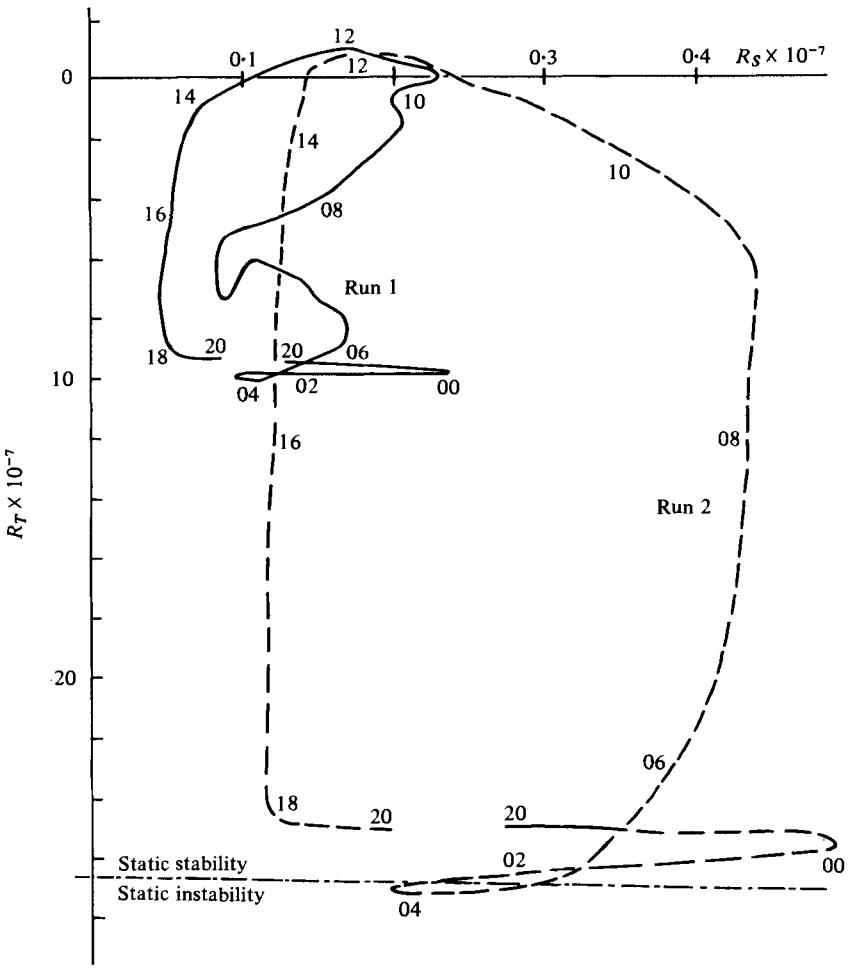

FIGURE 5. Rayleigh stability diagrams for second day of runs 1 and 2, at 1 m depth. Solid curve: run 1 (θ = 900). Broken curve: run 2 (θ = 0).

slightly lower rate of salt loss. By the end of the run, the maximum difference in surface σ_t between runs 1 and 3 is about 0·01. Owing to its similarity to that of run 1, σ_t from run 3 is not shown.

The trend toward lighter water is a result of the predicted decrease in salt content, and the slight modulation is the result of the strong diurnal heating cycle. This modulation in σ_t is also perceptible in the observed surface data.

For both simulations, Rayleigh numbers were calculated at all depths included in the integrations, and these indicate whether or not convective instabilities are present, and thus whether or not double-diffusive convection is possible.

Figures 5, 6 and 7 contain graphs of the movement of the point R_S, R_T on the R_S, R_T plane, for 1, 8, and 15 m, respectively. The scales of R_S and R_T have been expanded differentially for each figure in order to best show the plotted data. Therefore, the relationship between R_S and R_T, although still linear, has been distorted in the three figures. The line of static stability is defined by

$$R_T = -R_S - R_P. \tag{37}$$

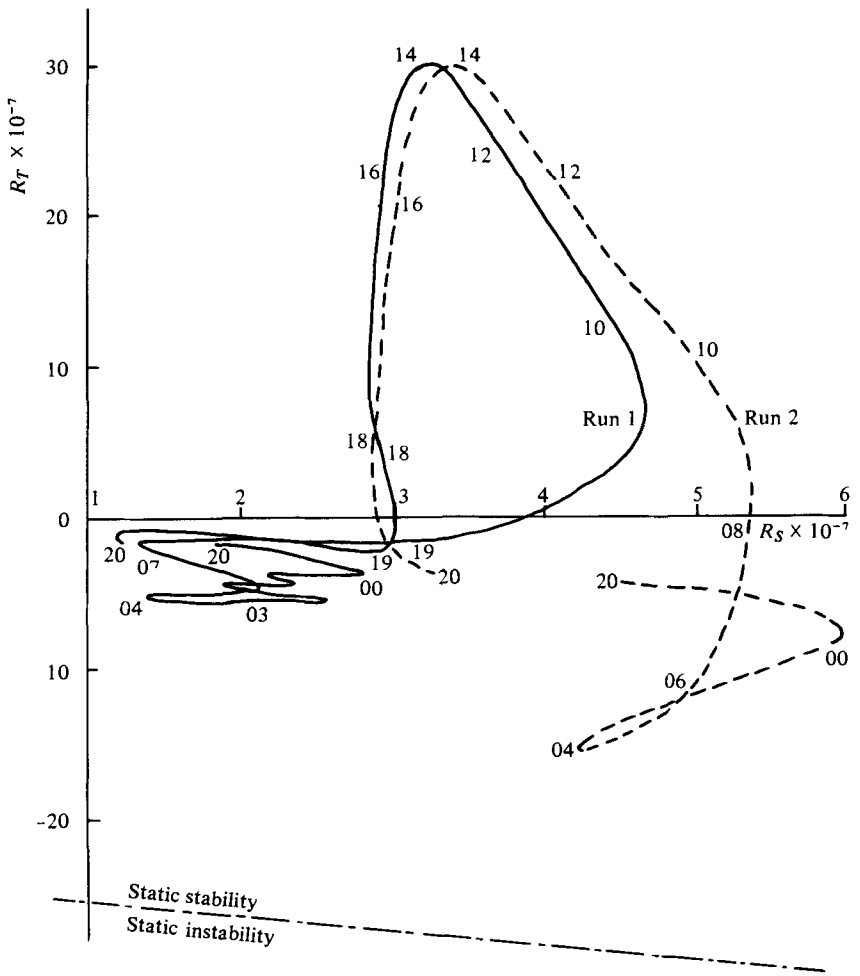

FIGURE 6. Same as figure 5, but for a depth of 8 metres.

This line is graphed in figures 5 and 6, but does not appear in figure 7. (It would pass to the left of that figure, so that all points on the region shown are statically stable.)

In each of the stability figures, two graphs are given: one for $\theta = 900$ (run 1) and the other for $\theta = 0$ (run 2). The stability results for run 3 (no precipitation) are identical in character to those of run 1 and thus are not given separately. The stability data plotted are for the same time interval (2000, 23 June 1969, to 2000 the next day) considered in the earlier figures for salinity, temperature, and σ_t. Time in hours is indicated at the appropriate locations on each curve. The starting point for each curve in the stability diagrams is labelled '20', as is the ending point. That the starting and ending points do not coincide is a manifestation of the slight heating trend and of the loss of salt due to horizontal advection. No stability diagrams are given for the observed data, since the slight irregularities in the observed profiles lead to wild excursions of the Rayleigh numbers, according to what particular depths are chosen, and also because observations are available only every three hours and interpolations are difficult. For the

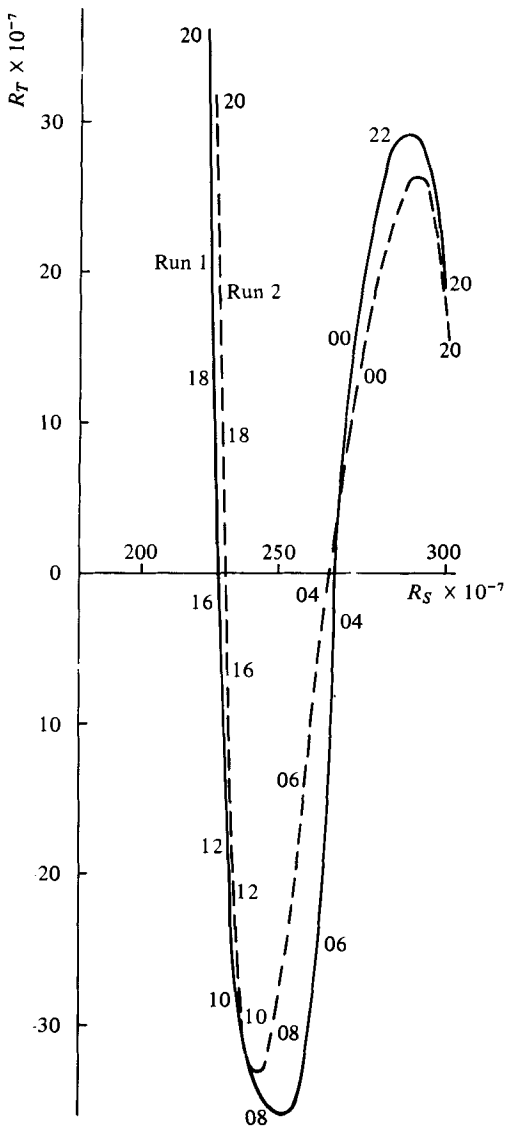

FIGURE 7. Same as figure 5, but for a depth of 15 metres.

simulations, of course, the profiles are generally smooth, and Rayleigh numbers can be calculated for every half-minute of modelled time.

The curve for run 2 in figure 5 shows that, from the start of the interval until about sunrise, there are changes in the near-surface salinity stability but that the temperature gradient stays roughly the same. The water at 1 m depth becomes statically unstable some time before 0300 and remains so until sunrise, at which time the surface water begins to warm. From sunrise until noon, the near-surface temperature stability increases, while the salinity stability changes slightly. In the afternoon, the temperature stability decreases and the salinity stability remains unchanged. After sunset (approximately 1800, labelled '18'), the thermal stability no longer changes, although

that for salinity does. The cycle for the next day is nearly identical, except for a slight migration to the left and a small compression of the entire pattern in the R_S direction. The curves never cross the R_T axis.

In the case of run 1, wherein convective instabilities were sensed and the diffusion rates were altered according to equations (32) to (35), the locus of Rayleigh stability is roughly the same as for run 2, except that the entire pattern is shrunk in both directions, indicating smaller surface gradients of both salinity and temperature. (The irregular excursion of R_S between 0600 and 0900 is unexplained, but has no bearing on the stability arguments here.) Note that the curves for runs 1 and 2 are nearly coincident during the two hours centred on noon. During this time, the temperature layering, by itself, has a stabilizing effect on the density, indicated by the fact that the curves move into the area for which $R_T > 0$. This, of course, is due to the strong solar heating at midday.

The loci of stability points for runs 1 and 2 for a depth of 8 m are given in figure 6. At this depth, the high thermal capacity of sea water causes the overall patterns to lag those of figure 5 (the surface stability plots) by some hours. The maximum thermal stability for a depth of 8 m is seen to occur at 1400, 2 hours later than for the surface water. The overall stability is stronger at 8 m depth than at the surface. The major differences between runs 1 and 2 in figure 6 occur only in the lower portion of the diagram, where the nighttime temperature stratification becomes convectively unstable.

The diurnal variations in stability at a depth of 15 m for runs 1 and 2 are nearly identical. In figure 7, the thermal gradient is seen to undergo wide, smooth changes over positive and negative convective stability, while the salinity gradient is very stable at all times. In fact, the slow decrease in R_S is nearly independent of time of day, and apparently reflects the gradual increase in the degree of mixing as the simulation progresses. Also, the net increase in R_T by the end of the cycle is indicative of the increasing stability of the average daily temperature gradient as the surface is warmed more rapidly than the deeper water.

All of the R_S, R_T plane shown in figure 7 is in the $R_E > 0$, or statically stable, no-convection regime, since the line of static stability would pass to the left and below the curves. This accounts for the similarity between the two curves.

6. Summary and conclusions

A numerical model for heat and salt in the upper ocean has been formulated and was used to predict the diurnal variations in thermohaline structure. A convective stability analysis was carried out at each time step, to enable modification of the vertical mixing coefficients for the succeeding time step. Three simulations were made: two with double-diffusive convection (the precipitation rate being set to zero for one of these) and one without. In a comparison with observed oceanic data, the simulations with double-diffusive convection produced better results. The simulation without double-diffusive convection had insufficient vertical mixing to remove near-surface static instabilities. It was thus shown that double-diffusive convection phenomena may be at work to stabilize the water column. This result is independent of the modelled precipitation rate.

The results demonstrate the necessity of including gradient information for both

temperature and salinity in modelling the diurnal heating cycle of the ocean. A similar result was obtained by Miller (1976) at a coarser vertical space scale and a seasonal time scale. The model of Foster (1971) did not include salinity gradient information and thus had no mechanism for preventing near-surface static instabilities.

In the present model, several parameters were adjustable: wind speed, air temperature and humidity, cloud cover, net solar radiation, vapour pressure, the horizontal gradients of temperature and salinity, horizontal currents, and precipitation rate. For all but the last two, observed data were used, and for these two parameters reasonable estimates were made. It is possible to choose values for the precipitation rate and the horizontal currents which would allow much closer agreement between observed and generated thermohaline structure. In fact, with a judicious choice of diurnal variation for precipitation rate and of currents, an exact replication of the observed temperature and salinity could have been forced. But such a reconstruction is not the purpose of the present study. Rather, the model was used for predicting the general diurnal heating cycle of the mixed layer, with particular emphasis placed on physical phenomena which, until now, had been neglected in oceanic models. Thus it is concluded that, with reasonable *a priori* estimates for certain input data, the diurnal heating cycle of the mixed layer is reasonably predicted by the model only if double-diffusive convection phenomena are included.

The model described here represents an attempt to model many of the processes known to be at work in the heating of the upper ocean. It is to be hoped that models developed in the future will include dynamic stability analysis and will go further by attempting to calculate the surface salinity more accurately. This will require much better precipitation measurements than are now available. Any study such as the present one would benefit greatly from accurate measurements of both horizontal currents at various depths and precipitation. It is felt that improved measurements of these parameters are needed in order to explain the very large excursions in observed salinity shown in figure 3. Then the input data for the model would be more complete, and presumably this would allow better predictions of the diurnal heating cycle in the mixed layer.

Appendix A. The numerical scheme

Equations (19) and (20) are solved numerically to give values of temperature and salinity at each grid point on a one-dimensional space grid, progressing over as many time steps as are needed to arrive at a prediction for a specified time.

The solution of equation (19) is begun with the splitting of $\partial T/\partial t$ into several components:

$$\frac{\partial T}{\partial t} = \left(\frac{\partial T}{\partial t}\right)_{\text{solar}} + \left(\frac{\partial T}{\partial t}\right)_{\text{advection}} + \left(\frac{\partial T}{\partial t}\right)_{\text{diffusion}} \tag{A 1}$$

with

$$\left(\frac{\partial T}{\partial t}\right)_{\text{solar}} = \frac{1}{c_p \rho}\frac{\partial}{\partial z}Q(z), \tag{A 2}$$

$$\left(\frac{\partial T}{\partial z}\right)_{\text{advection}} = -\left(u_x\frac{\partial T}{\partial x} + u_y\frac{\partial T}{\partial y}\right), \tag{A 3}$$

and

$$\left(\frac{\partial T}{\partial t}\right)_{\text{diffusion}} = \frac{\partial}{\partial z} K_T \frac{\partial T}{\partial z}. \tag{A 4}$$

Likewise,

$$\frac{\partial S}{\partial t} = \left(\frac{\partial S}{\partial t}\right)_{\text{advection}} + \left(\frac{\partial S}{\partial t}\right)_{\text{diffusion}} \tag{A 5}$$

with

$$\left(\frac{\partial S}{\partial t}\right)_{\text{advection}} = -\left(u_x \frac{\partial S}{\partial x} + u_y \frac{\partial S}{\partial y}\right) \tag{A 6}$$

and

$$\left(\frac{\partial S}{\partial t}\right)_{\text{diffusion}} = \frac{\partial}{\partial z} K_S \frac{\partial S}{\partial z}. \tag{A 7}$$

u_x and u_y are the eastward and northward components of current velocity, respectively. K_T, K_S, c_p, ρ and Q are calculated at each time step, while the horizontal velocity and gradient terms are treated as constants in time but are depth dependent. Time step is designated by i; space step by j. Δt is the size of the time step, 30 s, as discussed below. The lower boundary (nominally at 50 m depth) is represented by $j = 1$ and the sea surface by $j = N$.

From (12) and (15), the sea surface values of T and S are found for each time step, using the boundary value method given by James, Smith & Wolford (1967), and the use of an additional grid point $j = N + 1$.

The alternating direction explicit (ADE) scheme of Saul'ev (Richtmyer & Morton 1967, p. 192; Roache 1972, p. 99) as applied by Katsaros (1969) is used for solving the diffusion equations (A 4) and (A 7) at grid points $j = 2$ to $j = N$.

The spectrum of solar energy is divided into M frequency bands, each with a probability density function P_m and an attenuation coefficient Γ_m. The probability density functions are taken from Jerlov (1966), and the attenuation coefficients are from Tyler & Preisendorfer (1962) for oceanic coastal water. The extinction coefficient is taken to be the sum of the absorption and scattering coefficients, both of which are assumed to be wavelength dependent. From equation (A 2) the source term for solar radiation in the temperature equation (9) is

$$\frac{1}{c_p \rho} \frac{\partial}{\partial z} Q(z). \tag{A 8}$$

Equating this to $(\Delta T/\Delta t)_{\text{solar}}$, and using the finite difference expression for equation (26),

$$\begin{aligned}\left(\frac{\Delta T}{\Delta t}\right)_{\text{solar}} &= \frac{1}{c_p \rho} \frac{1}{\Delta z} \sum_{m=1}^{M} P_m [e^{-\Gamma_m (z+\Delta z)} - e^{-\Gamma_m z}] Q(0) \\ &= \frac{1}{c_p \rho} \frac{1}{\Delta z} \sum_{m=1}^{M} F_m(z),\end{aligned} \tag{A 9}$$

where

$$F_m(z) = [e^{-\Gamma_m (z+\Delta z)} - e^{-\Gamma_m z}] p_m Q'_m(0). \tag{A 10}$$

Following the calculation of $(\Delta T/\Delta t)_{\text{solar}}$, $(\Delta T/\Delta t)_{\text{advection}}$, and $(\Delta T/\Delta t)_{\text{diffusion}}$ for the current time step i for each grid point j, the incremental changes in temperature and salinity are estimated:

$$\Delta T_{\text{solar}} = \left(\frac{\Delta T}{\Delta t}\right)_{\text{solar}} \Delta t, \tag{A 11}$$

$$\Delta T_{\text{advection}} = \left(\frac{\Delta T}{\Delta t}\right)_{\text{advection}} \Delta t, \tag{A 12}$$

$$\Delta T_{\text{diffusion}} = \left(\frac{\Delta T}{\Delta t}\right)_{\text{diffusion}} \Delta t. \tag{A 13}$$

These are then added together to determine ΔT_j, which is added to T_j^{i-1} from the previous time step to obtain T_j^i, $1 \leqslant j \leqslant N+1$.

Conservation of heat was used as an index of quality for the overall scheme. This is a test for the numerical solution of the entire equation (9). An index ϵ is defined by

$$\epsilon = \frac{Q_{\text{rhs}} - Q_{\text{lhs}}}{-\int_0^\tau Q_f \, dt}, \tag{A 14}$$

where Q_{rhs} and Q_{lhs} are the right- and left-hand sides, respectively, of equation (18). Q_{rhs} is the total amount of heat added to the water column by solar heating, surface cooling, and horizontal advection, for $t = 0$ to $t = \tau$. Q_{lhs} is the net heat gain actually experienced by the modelled water column, over the same time interval. The denominator of equation (A 14) is the cumulative heat lost from the water to the air.

Calculation of ϵ over several days' simulation revealed that ϵ appears to consist of two components: one constant in time and independent of Δt, and one which causes an increase in error during sunlight hours and dependent on Δt. Time step sizes of 15, 30, and 60 s were tried, with best results seen for $\Delta t = 30$ s. For that time step size, ϵ never exceeded 4×10^{-3}, and the total heat deficit at the end of the 48 hours was only 2 cal cm^{-2}. This is more than two orders of magnitude smaller than the amount of heat which had been transferred from the sea to the atmosphere during the 48 hours. Because of this, and because it affords numerical stability and adequate convergence, 30 seconds was chosen as the time step for this model.

The numerical scheme was found to be stable, consistent with the diffusion equation, convergent, and sufficiently accurate to allow oceanographic interpretation.

Appendix B. Density and specific heat calculations

At each time step, σ_t is calculated with the method of Friedrich & Levitus (1972), c_p from that of Fofonoff (1962), and the latent heat of evaporation, L, from Sverdrup *et al.* (1942).

The coefficients of thermal and solutal expansion needed in the calculation of the Rayleigh numbers are determined by

$$\alpha = -\frac{1}{\rho_0}\frac{\partial \rho}{\partial T} = -\frac{1}{\rho_0}\frac{\partial \rho}{\partial \sigma}\frac{\partial \sigma}{\partial T} \tag{B 1}$$

and

$$\beta = \frac{1}{\rho_0}\frac{\partial \rho}{\partial S} = \frac{1}{\rho_0}\frac{\partial \rho}{\partial \sigma}\frac{\partial \sigma}{\partial S}, \tag{B 2}$$

using $\partial\sigma/\partial T$ and $\partial\sigma/\partial S$ from the Friedrich & Levitus formulation.

θ	K (m^2 min^{-1})	t (s)
0	0·001	10440 (= 2 h 54 min)
300	0·020	250
600	0·399	130
900	0·594	80
1200	0·790	60
2400	1·580	30

TABLE 1. K and t for various values of θ

Appendix C. Determination of the double-diffusive mixing parameter

From equations (31) and (34), it is seen that an increase in θ yields an increase in K'_{mT} and K'_{mS}, the effective convective diffusiveness for heat and salt respectively. Increased diffusiveness, in turn, causes greater vertical exchange rates of heat and salt. With the greater exchange rates, it is less likely that the numerical model will develop static instabilities. The temperature and salinity profiles generated at each time step are tested for regions of possible convective instabilities. Using the definitions presented in § 2 above, these regions, although statically stable, are actually marginally stable. Thus, they could become statically unstable were it not for the added exchange provided by double-diffusive convection. The added exchange tends to stabilize the water column.

It is easily shown that for a given length scale z, any diffusiveness K has associated with it a time scale t, where

$$t \sim z^2/K. \tag{C 1}$$

Thus the time scale is seen to be inversely proportional to the diffusiveness. A numerical experiment was performed by observing the time needed to remove an observed static instability, using various values of θ. The initial condition consisted of profiles of observed salinity and temperature which resulted in a density inversion of about 4×10^{-6} g cm^{-3} over a vertical extent of two metres. Table 1 lists the values of θ that were used in several diffusion simulations, with the values of K and the time required for stabilization of the water column. A time step of 30 s was used. The time needed for removal of the static instability is seen to obey equation (C 1) fairly well. Additional runs for $\theta = 1200$ and 2400 were made with a 10 s time step, with no change in results.

Following the arguments given in § 2 for the estimation of a minimum period for unstable convection in the upper ocean, $\theta = 900$ was chosen as appropriate. This gives a removal time of 80 s, which allows instabilities to be removed in time intervals somewhat smaller than the periods suggested in § 2. Small θ would give removal times much larger than those periods, and larger θ would result in removal intervals approaching the time step size of the model.

Support for this study was provided by the Defense Advanced Research Projects Agency under contract N00014-75-C-0777, monitored by the Office of Naval Research. Portions of this paper were used as part of a Ph.D. dissertation submitted to the faculty of Old Dominion University.

The author is indebted to C. E. Grosch, who, as chairman of the dissertation

committee, offered many stimulating ideas for the formulation of the model, and provided extensive help in the preparation of this manuscript.

Discussions and correspondence with C. A. Jacobs and with Rory O. R. Y. Thompson are also gratefully acknowledged.

This is a contribution of the Agricultural Experiment Station, Cook College, Rutgers University, New Brunswick, New Jersey 08903.

REFERENCES

CRAPPER, P. F. & LINDEN, P. F. 1974 The structure of turbulent density interfaces. *J. Fluid Mech.* **65**, 45–63.

DELNORE, V. E. 1972 Diurnal variation of temperature and energy budget for the oceanic mixed layer during BOMEX. *J. Phys. Oceanog.* **2**, 239–247.

DELNORE, V. E. & MCHUGH, J. 1972 *BOMEX Period III Upper Ocean Soundings.* Nat. Oceanic and Atmospheric Admin. Washington: U.S. Dept. of Commerce.

DIETRICH, G. 1963 *General Oceanography.* New York: Interscience.

ELLIOTT, G. W. 1974 Precipitation signatures in sea surface layer conditions during BOMEX. *J. Phys. Oceanog.* **4**, 498–501.

FOFONOFF, N. P. 1962 Physical properties of sea water. In *The Sea* (ed. M. N. Hill), pp. 3–30. New York: Interscience.

FOSTER, T. D. 1971 A convective model for the diurnal cycle in the upper ocean. *J. Geophys. Res.* **76**, 666–675.

FRIEDRICH, H. & LEVITUS, S. 1972 An approximation to the equation of state for sea water, suitable for numerical models. *J. Phys. Oceanog.* **2**, 514–517.

FRIEHE, C. A. & SCHMITT, K. F. 1976 Parameterization of air-sea interface fluxes of sensible heat and moisture by the bulk aerodynamic formulas. *J. Phys. Oceanog.* **6**, 801–809.

GARGETT, A. E. 1976 An investigation of the occurrence of oceanic turbulence with respect to fine structure. *J. Phys. Oceanog.* **6**, 139–159.

GARWOOD, R. W. 1977 An oceanic mixed layer model capable of simulating cyclic states. *J. Phys. Oceanog.* **7**, 455–468.

HUPPERT, H. E. 1972 Double-diffusive convection. In Notes on the 1972 Summer Study Program in Geophysical Fluid Dynamics, vol. I. Ref. no. 72–79 (Unpublished manuscript) Woods Hole Oceanographic Institution.

HUPPERT, H. E. & TURNER, J. S. 1972 Double-diffusive convection and its implications for the temperature and salinity structure of the ocean and Lake Vanda. *J. Phys. Oceanog.* **2**, 456–461.

JACOBS, C. A. 1978 Numerical simulations of the natural variability in water temperature during BOMEX using alternative forms of the vertical eddy exchange coefficients. *J. Phys. Oceanogr.* **8**, 119–141.

JACOBS, C. A. & PANDOLFO, J. P. 1974 A description of a general three-dimensional numerical simulation model of a coupled air–water and/or air–land boundary layer, vol. I. *The centre for the Environment and Man, Inc.*, Rep. no. 4131-509*a*.

JAMES, M. L., SMITH, G. M. & WOLFORD, J. C. 1967 *Applied Numerical Methods for Digital Computation with FORTRAN.* International Textbook, Scranton.

JERLOV, N. G. 1966 *Optical Oceanography.* Amsterdam: Elsevier.

KATSAROS, B. C. 1969 Temperature and salinity of the sea surface with particular emphasis on effects of precipitation. Ph.D. thesis, University of Washington.

KITAIGORODSKIY, S. A. 1961 On possibioity of theoretical calculation of vertical temperature profile in upper layer of the sea. *Bull. (Izv.) Acad. Sci. U.S.S.R., Geophys. Ser.* **3**, 313–318.

LANDIS, R. C. 1971 Early BOMEX results of sea surface salinity and Amazon River water. *J. Phys. Oceanog.* **1**, 278–281.

MADSEN, O. B. 1977 A realistic model of the wind-induced Ekman boundary layer. *J. Phys. Oceanog.* **7**, 248–255.

MALKUS, J. S. 1962 Large-scale interactions. In *The Sea* (ed. M. N. Hill), pp. 88–294. New York: Interscience.

MAMAYEV, O. I. 1958 The influence of stratification on vertical turbulent mixing in the sea. *Bull. (Izv.) Acad. Sci. U.S.S.R., Geophys. Ser.* **7**, 870–875.

MAZEIKA, P. A. 1973 Circulation and water masses east of the lesser Antilles. *Deut. Hydrografische Zeit.* **26**, 49–73.

METCALF, W. G. 1968 Shallow currents along the northeastern coast of South America. *J. Mar. Res.* **26**, 232–243.

MILLER, J. R. 1976 The salinity effects in a mixed layer ocean model. *J. Phys. Oceanog.* **6**, 29–35.

NEWMAN, F. C. 1976 Temperature steps in Lake Kivu: a bottom-heated saline lake. *J. Phys. Oceanog.* **6**, 157–163.

OSTAPOFF, F. & WORTHEM, S. 1974 The intradiurnal temperature variation in the upper ocean. *J. Phys. Oceanog.* **4**, 601–612.

PALM, E. 1975 Nonlinear thermal convection. *Ann. Rev. Fluid Mech.* **7**, 39–62.

PANDOLFO, J. P. & JACOBS, C. A. 1972 Numerical simulations of the tropical air-sea planetary boundary layer. *Boundary-Layer Met.* **3**, 15–46.

PAULSON, C. A., LEAVITT, E. & FLEAGLE, R. G. 1972 Air-sea transfer of momentum, heat, and water determined from profile measurements during BOMEX. *J. Phys. Oceanog.* **2**, 487–497.

PHILLIPS, O. M. 1966 *The Dynamics of the Upper Ocean.* Cambridge University Press.

PIERSON, W. J. 1964 The interpretation of wave spectrums in terms of the wind profile instead of the wind measured at a constant height. *J. Geophys. Res.* **24**, 5191–6204.

RICHTMYER, R. D. & MORTON, K. W. 1967 *Difference methods for Initial-Value Problems*, 2nd edn. New York: Interscience.

RYTHER, J. H., MENZEL, D. W. & CORWIN, N. 1967 Influence of the Amazon River outflow on the ecology of the western tropical Atlantic. I. Hydrography and nutrient chemistry. *J. Mar. Res.* **25**, 69–83.

ROACHE, P. J. 1972 *Computational Fluid Dynamics.* Hermosa.

SANFORD, T. E. 1972 Simulation of a one-dimensional model of an undisturbed air–sea boundary layer. *Proc. 1972 Summer Computer Simulation Conf.*, San Diego, pp. 895–902.

SHIRTCLIFFE, T. G. L. 1969*a* An experimental investigation of thermosolutal convection at marginal stability. *J. Fluid Mech.* **35**, 677–688.

SHIRTCLIFFE, T. G. L. 1969*b* The development of layered thermosolutal convection. *Int. J. Heat Mass Transfer* **12**, 215–222.

TURNER, J. S. 1965 The coupled turbulent transports of salt and heat across a sharp density interface. *Int. J. Heat Mass Transfer* **8**, 759–767.

TURNER, J. S. 1973 *Buoyancy Effects in Fluids.* Cambridge University Press.

TURNER, J. S. & STOMMEL, H. 1964 A new case of convection in the presence of combined vertical salinity and temperature gradients. *Proc. U.S. Acad. Sci.* **52**, 49–53.

TYLER, J. E. & PREISENDORFER, R. W. 1962 Light. In *The Sea* (ed. M. N. Hill), pp. 397–451. Wiley-Interscience.